Comparing Bio-Tribocorrosion of Selective Laser Melted Titanium-25%Niobium and Conventionally Manufactured Ti-6Al-4V in Inflammatory Conditions

V. Chakkravarthy, P. Manojkumar, M. Lakshmanan, K. Eswar Prasad, Rucha Dafale, V. Chitra Vadhana, R.L. Narayan

PII: S0925-8388(23)01155-6

DOI: https://doi.org/10.1016/j.jallcom.2023.169852

Reference: JALCOM169852

To appear in: *Journal of Alloys and Compounds*

Received date: 15 September 2022
Revised date: 11 March 2023
Accepted date: 27 March 2023

Please cite this article as: V. Chakkravarthy, P. Manojkumar, M. Lakshmanan, K. Eswar Prasad, Rucha Dafale, V. Chitra Vadhana and R.L. Narayan, Comparing Bio-Tribocorrosion of Selective Laser Melted Titanium-25%Niobium and Conventionally Manufactured Ti-6Al-4V in Inflammatory Conditions, *Journal of Alloys and Compounds,* (2023) doi:https://doi.org/10.1016/j.jallcom.2023.169852

Journal of Alloys and Compounds, Volume 952, August 2023, Article number 169852
DOI:10.1016/j.jallcom.2023.169852

Comparing Bio-Tribocorrosion of Selective Laser Melted Titanium-25%Niobium and Conventionally Manufactured Ti-6Al-4V in Inflammatory Conditions

V. Chakkravarthy [1,8*], P. Manojkumar [2], M. Lakshmanan [3], K. Eswar Prasad [4], Rucha Dafale [5], V. Chitra Vadhana [6], R.L. Narayan [7*]

[1] Welding and Additive Manufacturing Centre, Cranfield University, Cranfield, Bedfordshire, MK43 0AL, United Kingdom.
[2] Department of Metallurgical and Materials Engineering, National Institute of Technology Tiruchirappalli, Tamilnadu, India.
[3] Department of Mechanical Engineering, Ramco Institute of Technology, Rajapalayam, India.
[4] Discipline of Metallurgy Engineering and Materials Science, Indian Institute of Technology Indore, Simrol, Indore 453552, India.
[5] Department of Physiology, Kasturba Medical College, Manipal, Udupi, India.
[6] Department of Pedodontics and Preventive Dentistry, Indian Hospital, Udumalaipettai, Tamilnadu, India.
[7] Department of Metallurgical and Materials Engineering, Indian Institute of Technology Delhi, Hauz Khas, New Delhi, India 110016.
[8] Department of Metallurgical and Materials Engineering, Indian Institute of Technology Madras, Tamilnadu, India.

*Corresponding authors: chakkravarthyv5@gmail.com[1], rlnarayan@iitd.ac.in[2].

Abstract

The present study aims to evaluate the biocompatibility and bio-tribocorrosion potential of selective laser melted (SLM) Titanium-25% Niobium (Ti-25Nb) alloy. Further the suitability of the Ti-25Nb implant was assessed by benchmarking with conventionally manufactured commercial Ti-6Al-4V implant. Pin on disk tests were performed on these alloys while submerging them in an acidic sodium lactate (ASL) medium. Simultaneously, the open circuit potential (OCV) of the two alloys were measured before, during and after sliding the indenter. Characterization of the surface morphology and composition after the test revealed that SLM fabricated Ti-25Nb exhibits superior wear resistance and hence has greater resistance to depassivation than commercial Ti-6Al-4V implant. Biocompatibility of the implants, in terms of cell adhesion, cell proliferation, osteogenic differentiation and Alkaline Phosphatase (ALP) activity were also studied on the surfaces of the worn alloys. Results indicate that the worn Ti-25Nb surface is more conducive for the healthy growth of cells and facilitates more pronounced ALP activity than that of Ti-6Al-4V, over a duration of 14 days. The superior bio-tribocorrosion performance and biocompatibility of Ti-25Nb is attributed to SLM induced development of compressive residual stresses, smoother worn surface, higher compactness of the Nb oxides over the alloy surface and negligible toxicity of Nb.

Keywords: Additive manufacturing; Bio-tribocorrosion; Titanium-Niobium alloy; Bio-toxicity; Metal oxidative stress.

List of Abbrevations

1. Titanium-25% Niobium (Ti-25Nb)
2. Selective Laser Melting (SLM)
3. Titanium- 6% Aluminum- 4% Vanadium (Ti-6Al-4V)
4. Acidic Sodium Lactate (ASL)
5. Open Circuit Potential (OCV)
6. Alkaline Phosphatase (ALP)
7. Beta Titanium (β-Ti)
8. Additive Manufacturing (AM)
9. Laser Powder Bed Fusion (LPBF)
10. Hydrogen Peroxide (H_2O_2)
11. Zentrales Melderegister (ZMR)
12. Single Pole (SP)
13. Open-Circuit Voltage Potential (OCP)
14. Inductively Coupled Plasma (ICP)
15. Atomic ForceMicroscopy (AFM)
16. X-ray diffraction (XRD)
17. Clonal Murine Cell (MC)
18. Damidino –Phenylindole (DAPI)
19. Confocal Laser Scanning Microscopy (CLSM)
20. Cell Counting Kit-8 (CCK-8)
21. Inductively Coupled Mass Impedance Spectroscopy (ICMP)
22. Analysis of variance (ANOVA)
23. Field Emission Scanning Electron Microscopy (FESEM)
24. Inverse Pole Figures (IPF)
25. Electron Backscatter Diffraction (EBSD)
26. Average Root Mean Square Roughness (Rq)

27. Energy Dispersive Spectroscopy (EDS)
28. X-ray Photo-Electron Spectroscopy (XPS)

1. Introduction

Ti-alloys, are popular candidates for load-bearing implant applications owing to their high strength-to-weight ratio, good biocompatibility and excellent corrosion resistance [1-4]. Of these, Ti-6Al-4V is the most popular one and is being commercially used as an implant material. The only concern with the use of Ti-6Al-4V as an implant material is that it does not have inherent tribocorrosion resistance, which in necessary for implants attached to joints. Bio-tribocorrosion resistance is specifically required for implants connected to joints because they undergo motion, which leads to metal-on-metal rubbing. This causes wear of the implant surface and releases metal debris inside the human body [5,6]. Mouthuy et.al., (2018), pointed out that the release / accumulation of metal debris/ metal oxide and ions triggers an inflammatory response around the surrounding local tissues and causes significant discomfort to the patient thereby limiting the tribological applications. Also prolonged exposure to metal ions causes allergic reactions such as septic shock, bone resorption, apoptosis of bone cells, increased oxidative stress levels, aseptic loosening, and even pseudotumor in the patient [7]. Moreover, the body fluids surrounding the worn surfaces of the implant initiates a corrosion attack on it, which deteriorates its load bearing ability. A revision surgery, which is required for replacing the damaged implant, poses a socio-economic burden to the patient's family and causes agony to the patient during the procedure.

The underlying reason for the poor bio-tribocorrosion resistance of Ti-6Al-4V is as follows. When Ti-6Al-4V is exposed to aqueous medium, it forms passive films of TiO_2, Al_2O_3, and V_2O_5 on the surface [8]. The passive films on the native surface degrade due to abrasion and oxidation during the relative motion of the surrounding joints. Ideally, the contact of the fresh surface with

the medium should trigger the formation of a fresh passive film, which protects it from further corrosion and wear. However, the kinetics of fresh passive film formation is sluggish, which makes the fresh surface vulnerable to intense wear and corrosion. Moreover, Al ions released from the surface during wear react severely with tissue in animals and cause neurological disorders and Alzheimer's disease [3]. This particular issue led to the exploration of other Ti alloys that can serve as an alternative to Ti-6Al-4V for implant applications. In this context, it was reported that the tribocorrosion resistance of Ti improves with the addition of β-Ti stabilizing elements such as Nb, Zr, Ta, and Mo [9,10]. However, of these, only Ti-Nb alloys, with 10-40 at % Nb, satisfy the bio-compatibility requirements of an implant as it possesses good cytocompatibility, ensures adhesion of osteoblast cells, and facilitates cell proliferation [10,11]. Also, the addition of Nb in Ti alloys can reduce the overall elastic moduli to match the human cortical bone. However, making implants out of Ti-Nb alloys is still challenging as they are hard and hence cannot be easily machined to intricate shapes.

This issue can be resolved by adopting additive manufacturing (AM) techniques, such as selective laser melting (SLM) or laser powder bed fusion (LPBF) to produce Ti-Nb implants. In the SLM technique, a desired shape or structure is directly manufactured by layer-by-layer melting and solidification of alloy powders over a retracting bed [12-16]. This process minimizes material wastage and is also equipped to handle intricacies in design and shape of an implant.

However, while there are studies on tribocorrosion resistance of conventionally manufactured Ti-Nb alloys such as Ti-12Nb, Ti-15Nb, Ti-35Nb and Ti-40Nb alloys [17,18]. There are none which investigate bio-tribocorrosion behaviour on SLM fabricated ones. To address this gap in literature, we investigate the bio-tribocorrosion behavior of a Ti-25Nb alloy that was fabricated via SLM and compare it with that of an implant grade, conventionally manufactured Ti-6Al-4V

alloy. This particular composition of the Ti-Nb alloy was chosen as it was readily available and the % of Nb is 10-40 at.%, which is within the acceptable range appropriate for bio-implant applications [9]. Also, it is crucial to determine an implant material's bio-inertness and corrosion behavior in the presence of an environment with high levels of oxidative stress, where the pH would typically range from (2 to 3.5). Pin on disk tests were conducted on both alloys after immersing them in acidic sodium lactate (ASL) solution, which has a pH ≈ 2 [19]. When the test was conducted the open circuit potential of surfaces were simultaneously measured to understand their dynamic passivation behavior during wear. Note that most bio-tribocorrosion studies on Ti-Nb alloys were performed only in ambient conditions using simulated body fluids that have a pH of ~6.5-7. However, we chose a solution with a much lower pH as we expect the implant to be exposed to a more acidic medium with pH ≈ 2 - 3.5 in inflammatory conditions. This is because the inflammatory response of the body to foreign objects involves the accelerated production of hydrogen peroxide (H_2O_2) by proinflammatory cytokines. As a result, the pH becomes ~2-3.5 at the implant site for the first three to four weeks after surgery, which in turn, exacerbates the tribocorrosion of the implant [7].

This is followed by characterization and chemical analyses of worn surfaces of SLM fabricated Ti-25Nb and implant grade Ti-6Al-4V. Then, to assess the biocompatibility of the two alloys, in-vitro MC3T3-E1 cell culture studies, ALP activity assay and ion release studies were performed. Results of these studies indicate that SLM fabricated Ti-25Nb not only exhibits better bio-tribocorrosion resistance than conventionally manufactured Ti-6Al-4V but its worn surfaces also has better biocompatibility. The reasons for better performance of the former is attributed to its higher wear resistance, higher passive film integrity, lower ion release rates and lower toxicity of Nb in the human body.

2. Materials and Methods

The Ti-25Nb (% wt) alloy was fabricated using a selective laser melting (SLM) machine (Model: Ren AM 500 M). In this process, high purity gas-atomized Ti-25Nb (> 99.9%) feedstock powders were used. The average diameter of the powders was ~40µm. The powders were blended in a planetary ball mill at a ball to mill ratio of 1:10 at 200rpm for 1h in an inert atmosphere. The component was then built using SLM over a pure 15 mm thick Ti substrate, which was preheated to 200°C. To achieve near isotropic material characteristics, 67.5° rotational scanning strategy [20] was adopted as shown in Fig. 1. Pilot experiments to evaluate the optimal process parameters. The effects of three printing parameters, i.e. scanning speed, angle of rotation and laser power on porosity and cracking were examined. The process parameters that lead to a fully dense (~99.9%) and crack free build are finally chosen for making samples [21-24]. The details of other process parameters are listed in Table 1.

A medical grade Zentrales Melderegister (ZMR®) femoral head, whose composition is Ti-6Al-4V, was procured from (Zimmer GmbH, Winterthur, Switzerland). According to the manufacturers manual the commercial implant used in this study was fabricated through the conventional casting route Thereafter, the implant was post-processed by shot peening, followed by a stress relieving heat treatment. Then the surface finishing is performed by polishing, anodization, sterilization, and cleaning [25, 26].

Table 1. Optimal process parameters for SLM fabrication of Ti-25Nb alloy

S.No	Process parameters	Range
1	Laser power (W)	180

2	Spot size (μm)	50
3	Layer thickness (μm)	35
4	Scanning speed (mm/s)	1200
5	Hatch distance (μm)	70
6	Build size (mm)	40
7	Atmosphere content	Pure Ar and O_2 <500 ppm
8	Sample dimension (mm)	450×350×400

For simulating an inflammatory environment, a corrosive agent that causes lactic acidosis, which is the most common inflammation mediator at the implant site, must be chosen. In our study we choose acidic sodium lactate (ASL) electrolyte, which contains lactic acid (pH ≈ 2), as the corrosive media to mimic the inflammatory environment. The ASL solution was freshly prepared by dissolving (0.1 M) sodium lactate and (0.1 M) of HCl in distilled water [19].

In most prosthesis, such as femoral implants, the femoral head or the component attached to the joint experience frictional contact and cause inflammation. For investigating tribocorrosion specifically in this region, plate of dimensions, 50 x 25 x 5 mm were extracted from the top (X-Y plane) of the Ti-25Nb build (which would correspond to the location of the femoral head) and Ti-6Al-4V femoral implant. Tribocorrosion experiments were performed on these SLM produced Ti-25Nb and Ti-6Al-4V plates, immersed in the ASL solution, using a pin on disk tribometer (Model: CETR UMT-1) at an oscillation frequency of 2 Hz, applied load 5 N, the stroke length of 2.5 mm, and sliding duration of 11000 seconds. The sliding duration is chosen to ensure that there is sufficient time for repassivation of the alloy surfaces. Before performing these tests, Ti-25Nb surfaces were electropolished. During the tribocorrosion test, a 10 mm diameter alumina ball slides over an area ~1 cm^2 on the alloy surfaces. The electrolytic cell comprises of standard hydrogen electrode as the reference electrode, working electrode (Ti-25Nb

or Ti-6Al-4V) (10mm × 10mm × 3mm), counter electrode (platinum wire). Data acquisition is done via a SP 150 Potentiostat and processed through EC-Lab software. Before performing tribocorrosion experiments, the working electrode was immersed in ASL solution for achieving stable open-circuit voltage potential (OCP). The OCP before, during, and after sliding is continuously recorded. Furthermore, the release of metal ions in the corrosion media during tribocorrosion experiments was quantified using an inductively coupled plasma-atomic emission spectrometer (ICP) (Model: AES Ultima expert, France). For repeatability, all the tribocorrosion experiments were repeated on three different samples. The grain orientation analysis was performed by EBSD measurements by choosing an acceleration voltage and a step size of 20 V and 0.4 μm respectively. Further the raw EBSD data was processed through TSL orientation imaging microscopy (OIM) analysis software. The worn surface was characterized using Field Emission Scanning Electron Microscopy (Model: FEI Quanta 200 HV). The worn topology was characterized through Atomic Force Microscopy (AFM) (Model: NTEGRA Prima). Hardness tests were performed on plates of both alloys using Matsuzawa MMT-X Vicker's hardness tester with an applied load of 200 gf with a dwell time of 10 s. Using the conventional X-ray diffraction (XRD) with $Sin^2\psi$ method, a XRD instrument (Proto-XRD, Canada) was used to measure residual stresses in SLM fabricated Ti-25Nb along the z direction [27-31]. The residual stress in the sample's depth was determined by removing the surface layer by layer using an electro-polishing method. The residual stress analysis was performed from the top layer towards the bottom layer (anti-parallel to the build direction). From the fabricated sample, a portion was sectioned from the top to the bottom layer for residual stress analysis. XRD was also used to map the phases in the two alloys. For this Cu-Kα radiation (λ = 1.541838 Å) with a Nickel filter was used as the X-ray source. The surface components of the both the materials after tribocorrosion

were observed using X-ray photoelectron spectroscopy (ULVAC, Japan) with Al-Kα (1486.6 eV) as an excitation source.

Furthermore, a biocompatibility assay was performed using MC3T3-E1 pre-osteoblasts cells that were cultured in 10% of Fetal Bovine serum and 100 μg/mL of streptomycin placed at a normal room temperature of 32°C in a humidified environment (95% O_2 and 5% CO_2). A fresh media was replaced every 2 days until it reaches 80% confluence. Later cells were seeded at a density of 1×10^4 cells/cm^2 on well sterilized plates of Ti-6Al-4V and Ti-25Nb. Later cells were stained with 4′,6-damidino-2-phenylindole (DAPI) and consistently monitored for (1d,3d,5d) using confocal laser scanning microscopy (CLSM) (Model: Zeiss LSM-510, Germany) to study the development of cytoskeleton and nuclei of MC3T3-E1 pre-osteoblasts cells. In addition, cell viability and cell proliferation were measured via a CCK-8 assay (Make: Thermo Fisher) kit using a microplate reader (Model: Infinite 200 Pro, Tecan) at a wavelength of 450 nm. Finally, osteogenic differentiation of MC3T3-E1 at early-stage was studied using an Alkaline Phosphatase (ALP) Activity assay Kit (Make: Beyotime). Cell adhesion and cell spreading were estimated with the aid of Image-Pro Plus 6.0 software. An in-vitro ion release test was conducted according to ISO 10993-12 2007 standards via inductively coupled mass impedance spectroscopy (ICMP). The statistics of ion release is analyzed with one-way analysis of variance (ANOVA) followed by Dunnett's multiple comparison test. Tests were performed inside two simulated body fluids, Hank's solution (pH≈ 6.5-7.2) and ASL solution (pH≈ 2) for 14 days.

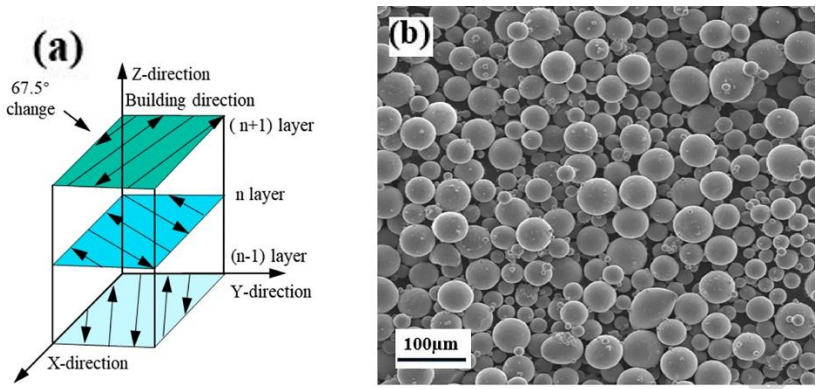

Fig. 1(a) Bidirectional deposition strategy with 67.5° rotational angle, FE-SEM of Ti-25Nb powder mixture.

3. Results and discussions

The EBSD inverse pole figures (IPF) of SLM fabricated Ti-25Nb along the Y-Z, X-Z and X-Y planes are shown in Fig. 2. In all planes, the microstructure consists of α+β plates that are arranged in the Widmanstätten basketweave morphology. Across the grain boundaries, the α+ β colonies have different growth orientations and have an average thickness of 2.6 ±0.4 µm. Moreover, the texture is random unlike that typically reported for α+β Ti alloys, which have a <0001> dominant texture [32]. These features are an outcome of the non-uniform thermal gradients in SLM fabrication. Following the melting of the Ti-25Nb powders, solidification begins with the formation of the β-grains. According to the Ti-Nb phase diagram, for the chosen composition of Nb, α+β are the room temperature equilibrium phases [33]. If the thermal gradient is uniform, the nucleation of the α+β lamellae begins at the boundaries, which is followed by their growth along the direction of the thermal gradient. However, given that the thermal gradients in SLM fabrication are non-uniform due to the 67.5° scan rotation strategy employed in the study, there can be multiple growth fronts for the α+β lamellae, which results in a basketweave or Widmanstätten microstructure.

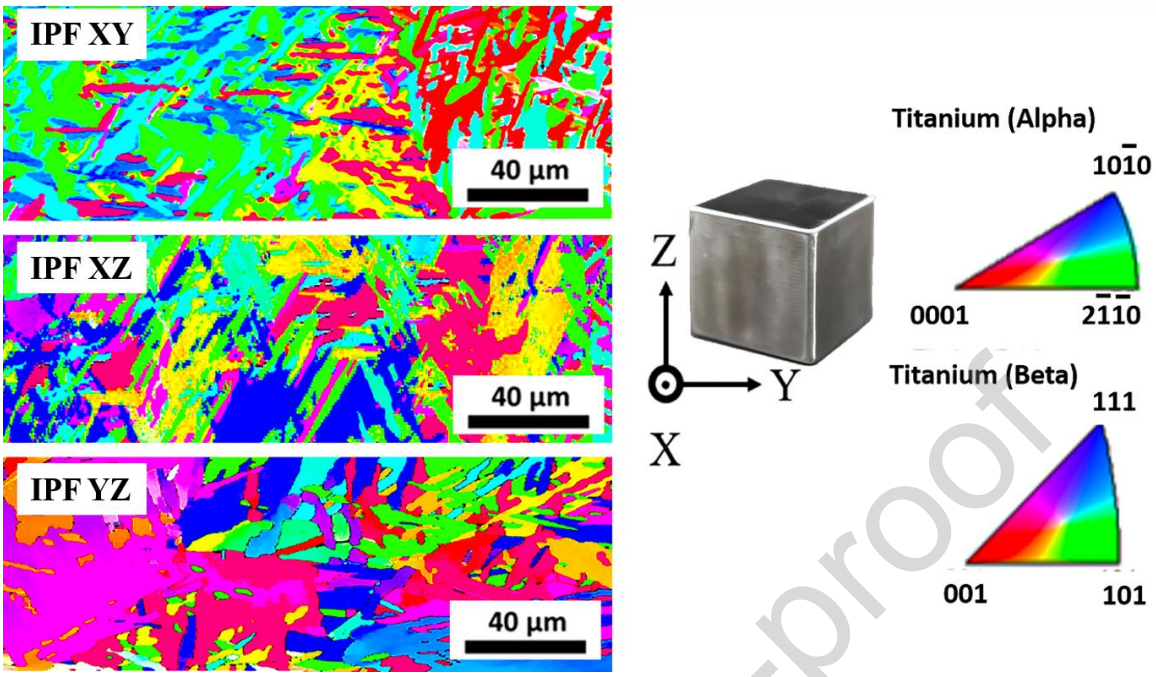

Fig. 2 Inverse pole figure maps of SLM fabricated Ti-25Nb alloy on Y-Z, X-Z, X-Y planes.

The representative microstructure of the wrought Ti-6Al-4V ZMR femoral implant is shown in Fig.S1. The summary of important microstructural features in it are as follows. This alloy has an equiaxed α+β microstructure with an average grain size of 45 µm. Grains are elongated in the longitudinal direction but are homogeneous in the transverse direction. The XRD scans of both alloys, shown in Fig. S2, confirm the presence of the α and β phase in both alloys.

Next, room temperature microhardness of SLM fabricated Ti-25Nb and implant grade Ti-6Al-4V are compared. Ti-25Nb has a uniform microhardness of 387±7 HV on the X-Z plane whereas that of Ti-6Al-4V is only 341 ± 9 HV. The higher hardness of the former is attributed to its finer α+β microstructure the difference in fabrication methods of the two alloys. Since Ti-25Nb undergoes rapid cooling during SLM, it has high residual stresses. Depending on the processing or surface treatment, residual stresses in metal implants can be either compressive or tensile. Tensile residual stresses in implants are generally undesirable as it promotes corrosion, wear, stress corrosion cracking and also makes it susceptible to fatigue damage [34, 35]. Alternately,

compressive residual stresses are beneficial as it hinders metal ion transfer in Ti alloys, which mitigates corrosion. Also, compressive residual stresses enhances the hardness, which in turn improves the wear resistance according to Archard's law [36, 37]

Therefore, in this study the effect of residual stress on bio-tribological performance was evaluated. In contrast, implant grade Ti-6Al-4V, which is conventionally manufactured, undergoes equilibrium cooling and hence has negligible residual stresses. To further quantify the residual stresses in SLM fabricated Ti-25Nb X-ray diffraction analysis is performed in it using the $Sin^2\psi$ method [37]. Fig. 3 shows the residual stress distribution in the alloy the from the top to bottom of the build, anti-parallel to the build direction.

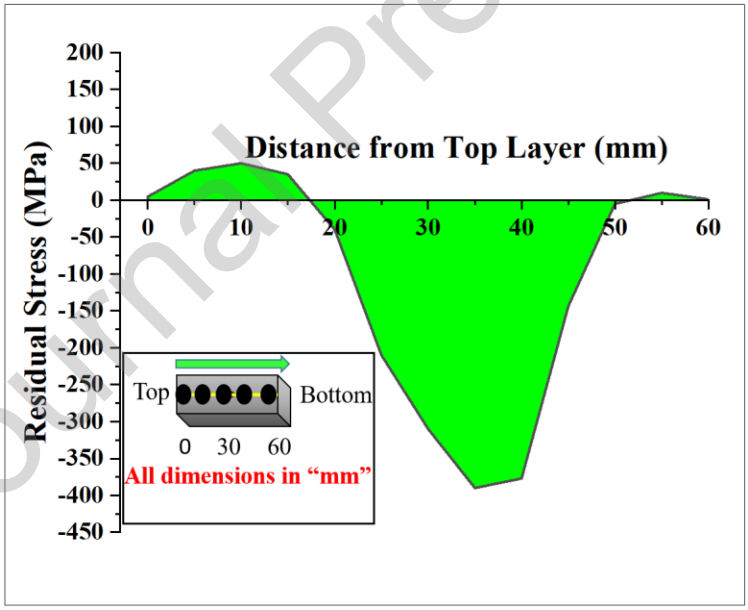

Fig.3. X-ray residual stress plots of SLM fabricated Ti-25Nb alloy.

The residual stress is -344MPa at the top of the build, which monotonically decreases with increasing distance from it and becomes 61MPa, at the bottom. The observed gradient in residual stress distribution is attributed to the variations in the thermal history in the build. As mentioned earlier, the rapid solidification of the Ti-25Nb melt during SLM leads to build-up of residual

stresses in the SLM fabricated layers. However, subsequent addition of layers also leads to heat accumulation in the build, which continuously relieves these stresses. However, the stress relief due to heat accumulation is not uniform throughout the build. Layers of material at the bottom of the build, which are exposed to heat for a longer time, undergo more stress relief than the top layer. Therefore, the top-most layer in the build has the highest compressive residual stresses, whereas the bottom is relatively stress-free. On the other hand, the residual stresses in implant grade Ti-6Al-4V are negligible owing to the absence of such thermal effects during their fabrication. In summary, the results of the microstructure and mechanical properties of SLM fabricated Ti-25Nb and implant grade Ti-6Al-4V indicate that both have an α+β microstructure. The former has a fine lamellar microstructure whereas that of the latter is coarse and equiaxed. Ti-25Nb has gradients in residual stresses from the top of the build, which is compressive, to negligible at the bottom. As a result of the fine grain sizes and compressive residual stresses, the top surface of SLM fabricated Ti-25Nb are harder than implant grade Ti-6Al-4V (whose hardness is 349 HV). The hardness profile measured from the top to bottom of the SLM printed Ti-25Nb, presented in Fig. S3, confirms the same.

Next, the results of the bio-tribocorrosion tests on SLM fabricated Ti-25Nb and implant grade Ti-6Al-4V were analyzed. The bio-tribocorrosion results of the two surfaces can be directly compared if they have similar initial average root mean square roughness, R_q. This is indeed the case as R_q of Ti-25Nb and Ti-6Al-4V is ≈ 8.5 ± 0.5μm and ≈ 7 ± 0.5μm, respectively, as shown in Fig. 4.

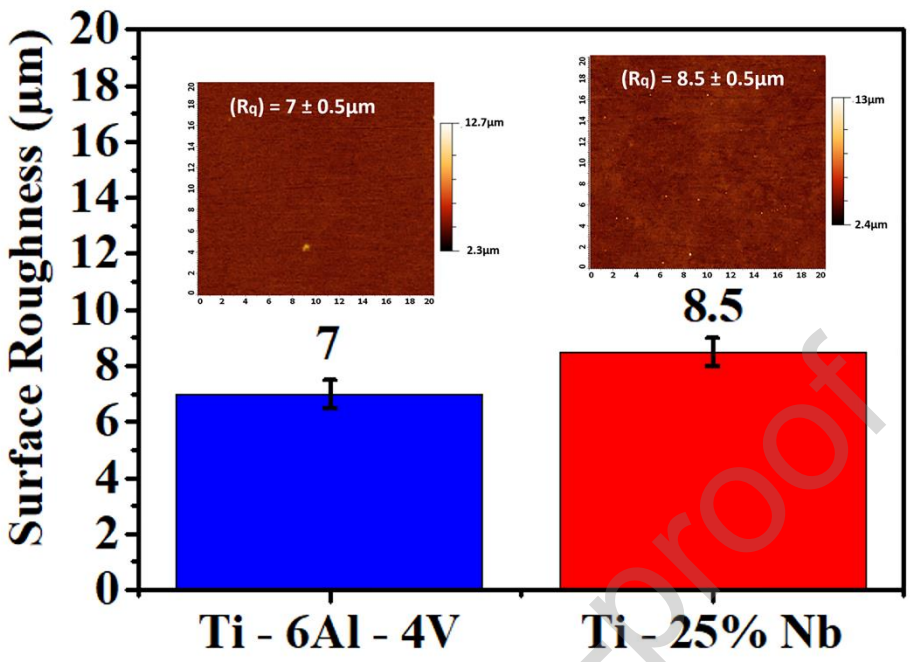

Fig. 4. AFM surface topology prior to tribocorrosion experiments.

Fig. 5 shows the variations of open circuit potential (OCP) with time, before, during, and after sliding experiments were performed on SLM fabricated Ti-25Nb and implant grade Ti-6Al-4V surfaces immersed in ASL solution. The OCP is initially -0.1 V for both surfaces. Once sliding starts at 2000 s, the corrosion potential on both surfaces drops from 0.1 V to -0.6 V. The drop in OCP is attributed to the removal of the passive oxide layer by the sliding indenter followed by electron transfer to the fresh exposed surfaces. With increasing sliding duration, the OCP continues to decrease on both alloy surfaces. However, the rate of drop in OCP on Ti-6Al-4V is steeper than that on Ti-25Nb. On the Ti-6Al-4V surface, the OCP at 6000 s is ~-0.9 V whereas that on Ti-25Nb it is ~-0.75 V. At the end of sliding, which is after 12000 s, Ti-6Al-4V and Ti-25Nb have OCP of ~-0.98 V and ~-0.88 V, respectively. After sliding ends, the OCP of Ti-6Al-4V gradually rises to -0.5 V but that of Ti-25Nb recovers more modestly to ~-0.6 V.

However, during sliding, the decrease in OCP is non-monotonic as it intermittently increases and decreases with increasing sliding duration, which manifests as serrations in the curves. The average magnitude of the OCP fluctuations on both surfaces are ~ 0.2 V. Although a characteristic period of the serrations could not be determined, each one occurs over a duration of 100-500 s. Overall, the OCP of implant grade Ti-6Al-4V drops to a much lower value than that on SLM fabricated Ti-25Nb during sliding of the pin over the surface.

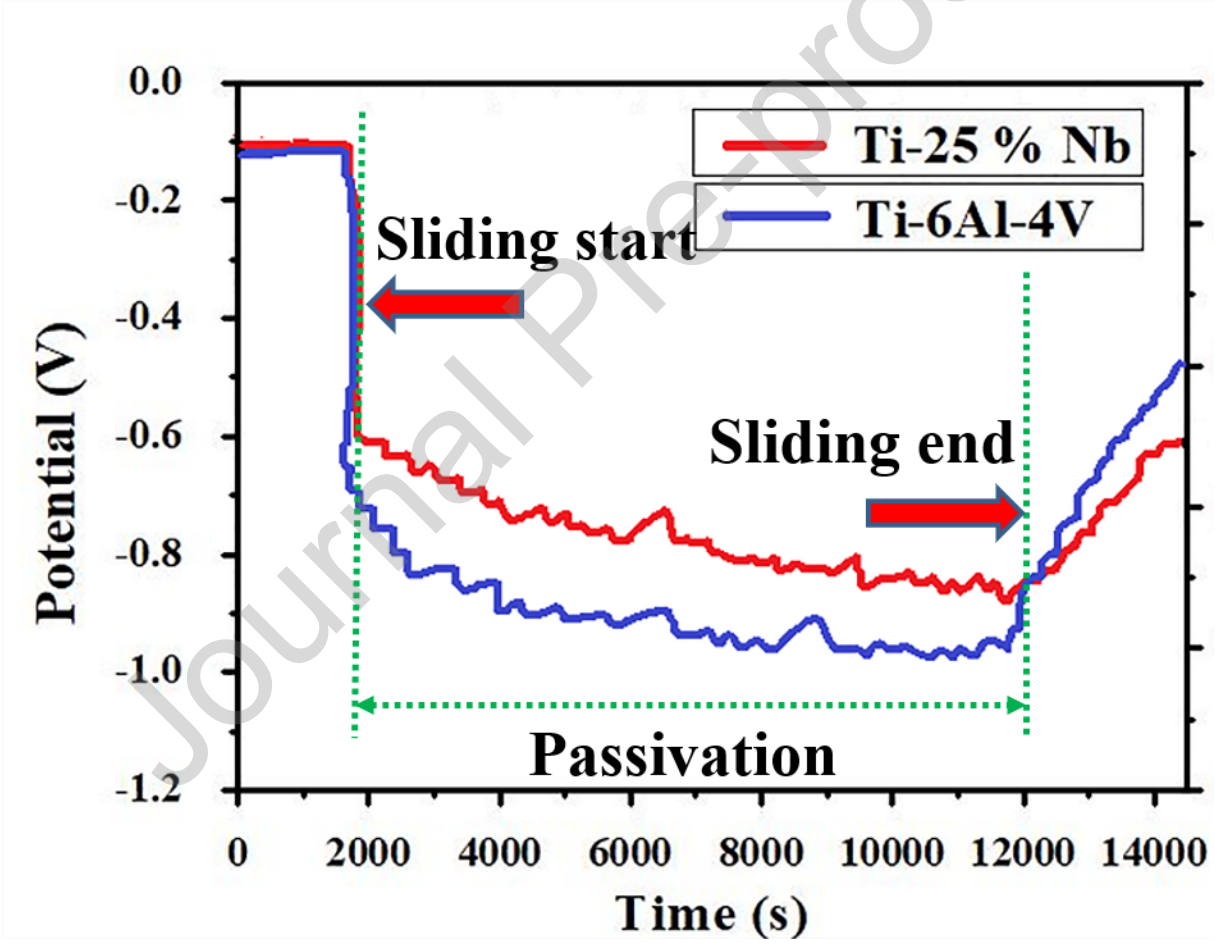

Fig. 5. Bio-tribocorrosion graph of Ti-6Al-4V and Ti-25Nb.

Further characterization of the worn surfaces of the two alloys is performed using AFM and FE-SEM. The FE- SEM images of implant grade Ti-6Al-4V and SLM fabricated Ti-25Nb are shown in Fig 6(a) and 6(b), respectively.

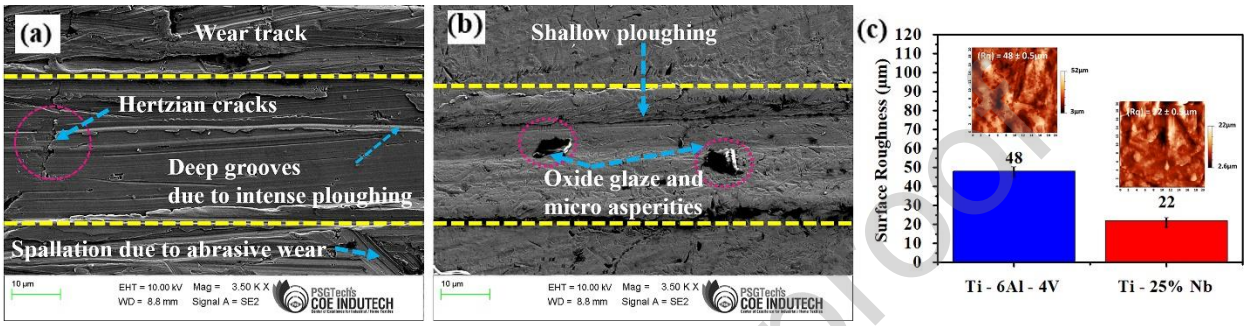

Fig. 6. (a) FE-SEM morphology of Ti-6Al-4V worn surfaces, (b) Worn morphology of Ti-25Nb alloy, (c) AFM surface roughness histograms of the worn Ti-6Al-4V and Ti-25Nb samples.

Deep grooves were observed on the Ti-6Al-4V surface, which indicated that they experienced intense ploughing. Additionally, their worn surface has deep grooves, Hertzian cracks, spalled material and hackle marks indicating intense plastic deformation and damage due to abrasion wear [38-39]. Alternately, Ti-25Nb undergoes relatively lesser wear damage as only shallow ploughing marks covered by oxide glaze and microscopic asperities were observed. Alberta et.al.(2023) reported a similar observation during bio-tribocorrosion of β-type Ti-Nb-Ga alloy [40].

The AFM images of Ti-25Nb and Ti-6Al-4V are shown in Fig. 6(c). Ti-6Al-4V surface has a relatively higher R_q of ~48 ± 0.5 µm compared to that of Ti-25Nb, which is only ~22 ± 0.5 µm. Similarly, the COF of the former is 0.31 whereas that of the latter is 0.25, which is consistent with the trend in R_q.

To understand the changes in chemistry of the surfaces after bio-tribocorrosion tests, their compositions are analyzed with energy dispersive spectroscopy (EDS). The EDS maps of Ti-6Al-4V and Ti-25Nb are shown in Fig. 7.

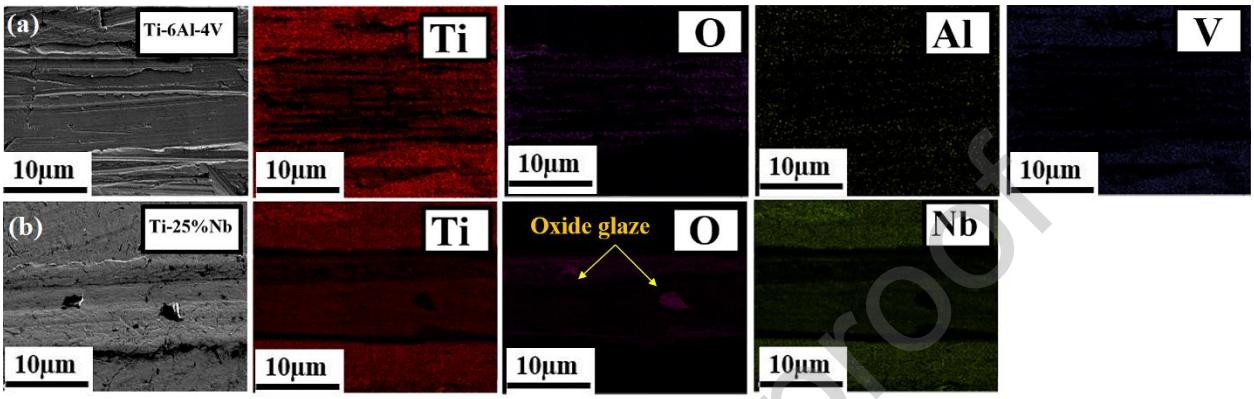

Fig. 7. EDS colour mapping of worn surfaces of Ti-6Al-4V alloy and Ti-25Nb.

Apart from the primary constituents of the alloys, the presence of oxygen was noted in both wear tracks. However, in Ti-25Nb, oxygen appears to be concentrated in the form of oxide glaze, whereas in Ti-6Al-4V it is a part of the streaks in the wear track.

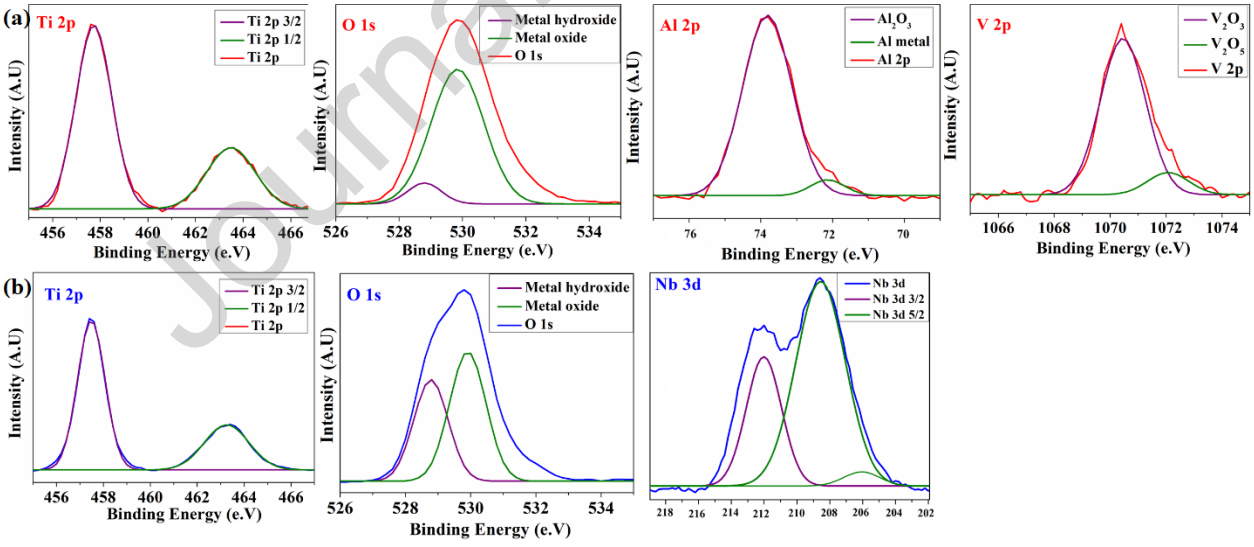

Fig. 8. XPS scans on passive film chemistry of Ti-6Al-4V alloy and Ti-25Nb alloy.

The resolution of EDS is limited, and further analysis of the elemental composition is performed using X-ray photo-electron spectroscopy (XPS). The XPS scans of the two bio-tribocorrosion

tested surfaces are shown in Fig. 9. Besides peaks of the primary constituents in both alloys, several oxide peaks were also observed. On the worn Ti-6Al-4V surface, peaks corresponding to TiO_2, Al_2O_3, V_2O_5 and V_2O_3 were observed. Alternately, peaks of TiO_2, Nb_2O_5 and Nb_2O_3 were detected in the worn tracks of Ti-25Nb. Note that in both worn surfaces, the presence of hydroxides and dissolved oxygen was also detected.

Based on these results, a detailed description of processes involved in bio-tribocorrosion of SLM fabricated Ti-25Nb and implant grade Ti-6Al-4V is as follows. Before sliding begins, the Ti-6Al-4V surface, exposed to the ASL solution, is covered with TiO_2, Al_2O_3, V_2O_5 and V_2O_3 passive films, whereas that of Ti-25Nb contains TiO_2, Nb_2O_5 and Nb_2O_3 passive films. These films prevent corrosion of the surface, which is evident from the initial low value of OCP ~ -0.1V. When the alumina ball begins sliding over the surfaces, these passive oxide films get eroded in both alloys and their fresh surfaces are exposed to the ASL solution. This leads to a galvanic coupling between the freshly exposed surface and its surroundings, where the former acts like the anode and the latter, cathode. The freshly exposed surfaces in each alloy releases metal ions and transfers electrons to the surrounding surfaces, which undergoes cathodic polarization. These events correspond to the initial steep drop in OCP measured on both alloys (see Fig. 5). The extent of the drop in OCP depends on the extent of removal of the oxide film, which in turn depends on its compactness and wear resistance. Given that the SLM fabricated Ti-25Nb is harder and has greater residual stresses than implant grade Ti-6Al-4V, its wear resistance is expected to be higher.

The shallower ploughing and lower roughness of the former compared to that of the latter (see Fig. 6) confirms the same. A higher wear resistance of SLM fabricated Ti-25Nb ensures lesser removal of the passive layer over its surface during sliding. The exposure of lesser fresh Ti-25Nb

surfaces compared to that of Ti-6Al-4V to ASL solution at the onset of sliding limits its cathodic polarization and mitigates the drop in its OCP (see Fig. 5).

After removal of the passive oxide layer, the difference in potential between it and the surrounding surface drives repassivation of the former, which manifests as a slight increase in the OCP. The repassivated films on both surfaces contains a mixture of constituent metal oxides and hydroxides that were identified in Fig. 8. However, the continuous sliding motion of the ball over the exposed surface keeps removing the oxide layer formed from passivation and again depassivates it, leading again to a decrease in OCP. The intermittent occurrence of electrochemically driven repassivation and wear induced depassivation leads to a fluctuating value of OCP, which manifests as serrations in the OCP curves of both alloys, as was observed in Fig. 5. After the end of sliding, depassivation ends and the passive oxide layer gradually forms over the worn surface, which manifests as an increase in the OCP of both alloys. SLM fabricated Ti-25Nb, owing to greater compressive residual stresses, also recovers to a lower OCP compared to that of implant grade Ti-6AL-4V. Compressive residual stresses in the former hinders the diffusion of oxygen and hydroxide ions into its surface. Diffusion of these ions is necessary for creating the passive oxide film on the alloy surface. Similar observations were reported by Rahmatian et.al.,(2023) and Cheraghali et.al., (2022) [41, 42]. The sluggish passive film formation kinetics of the oxide film on the surface of Ti-25Nb, leads to an underwhelming anodic shift of its OCP compared to that of Ti-6Al-4V.

Another factor that contributes to the superior tribo-corrosion resistance of Ti-25Nb to that of Ti-6Al-4V is the differences in the chemistries of their films. Note that amongst the passive oxide films on Ti-6Al-4V, TiO_2 is most stable, whereas Al_2O_3, V_2O_5 and V_2O_3 films are relatively less stable [33]. As a result, Ti-6Al-4V alloy had undergone a high magnitude of abrasive wear

leading to in-depth grooves over the sliding surface and corrosion which discharges metal ions into the ASL solution. However, Nb_2O_5 and Nb_2O_3 passive films are as stable as TiO_2 passive films and do not undergo abrasion during wear as easily.

Besides bio-tribocorrosion resistance, a potential implant material needs to possess good cytocompatibility and osteointegration abilities. To examine and compare these aspects in Ti-6Al-4V and Ti-25Nb, in-vitro MC3T3-E1 cell culture studies were performed on them. The cell viability and proliferation were estimated on the worn alloy surface for durations of 1, 3 and 5 days and quantified by CCK-8 assay and optical density (OD) measurements via CLSM. For the first 3 days, the cell density on Ti-6Al-4V and Ti-25Nb surfaces increased steadily but had a similar OD of 0.21 and 0.23 respectively. However, on the 5th day of exposure, Ti-25Nb alloy exhibits superior cell proliferation of 1.31 ($p < 0.05$) compared to that of Ti-6Al-4V, which is only 1.15. This is evident in the CLSM images of the SLM fabricated Ti-25Nb and Ti-6Al-4V after the 5th day of cell culture studies, which is shown in Fig. 9(a).

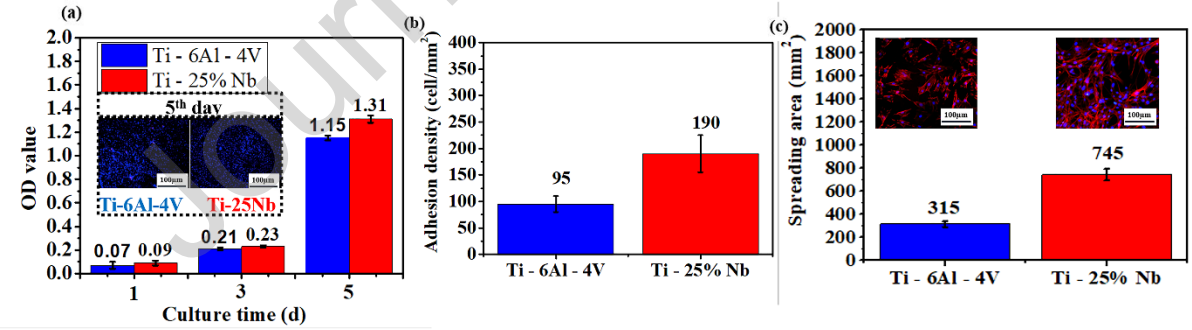

Fig. 9 (a) Cell viability assay, (b) Cell adhesion, (c) Cell spreading of Ti-6Al-4V and Ti-25Nb alloy.

To obtain a better understanding of the alloy surface- cell interaction, the viable cells that were added to the two alloy surfaces were viewed through CLSM. To distinguish the nucleus and actin cytoskeleton, they were stained with rhodamine-conjugated phalloidin and DAPI, which give a

red and blue contrast, respectively. The fluorescent images of Ti-25Nb and Ti-6Al-4V are displayed in Fig. 9(b). The traces of the elongated cytoskeleton of MC3T3-E1 cells adhered over the alloy surfaces and the spreading of filopodia and lamellipodia were observed. After 5 days of exposure, while both the surfaces exhibited cytoskeleton development, Ti-25Nb exhibited a denser cellular adherence of 190 ± 30 cell/mm^2, whereas that on Ti-6Al-4V implant is only 95 ± 22 cell/mm^2.

Furthermore, the cell spreading area on Ti-25Nb alloy was ~745 ± 50 μm^2 which is two-fold higher than that on the commercial Ti-6Al-4V.

Cell adhesion, cell migration and other aspects of cell responses depend on roughness of the implant surfaces. A cell can adhere to its environment by increasing the number of contact points to potentially assist cell elongation. The adhesion force of cells is governed by the Lifshitz-van der Waals theory of attractive forces and electrostatic interactions [43]. It was thus hypothesized that uneven surfaces, such as the grooves and tear ridges present in the worn Ti-6Al-4V surface (Rq ≈ 48 ± 0.5 μm), are not ideal for maintaining good contact with the boundaries of cells. This leads to constrained growth of a sizeable proportion of the cells in localized areas of the alloy surface, as was seen in Fig. 9. In contrast, the less abraded Ti-25Nb surface, which has a much lower R_q ~ 22 ± 0.5μm exhibits greater adhesion and more uniform cell distribution owing to more intimate contact with the cells. The optimal roughness of Ti-25Nb surface is also conducive for stretching of cell membranes, elongation of the cytoskeleton, and hierarchical response of cell contractility.

To understand the performance of the two alloys in terms of osteogenesis, early cell differentiation assessed through an ALP activity assay. ALP is an important enzyme that active in an alkaline environment (pH ~6-10) and produces free phosphate, which in turn facilitates

bone mineralization [44]. Therefore, increased ALP activity is favorable for healing bones close to the implant. The ALP activity in the presence of wear-tested Ti-25Nb and Ti-6Al-4V was assessed and compared for 14 days.

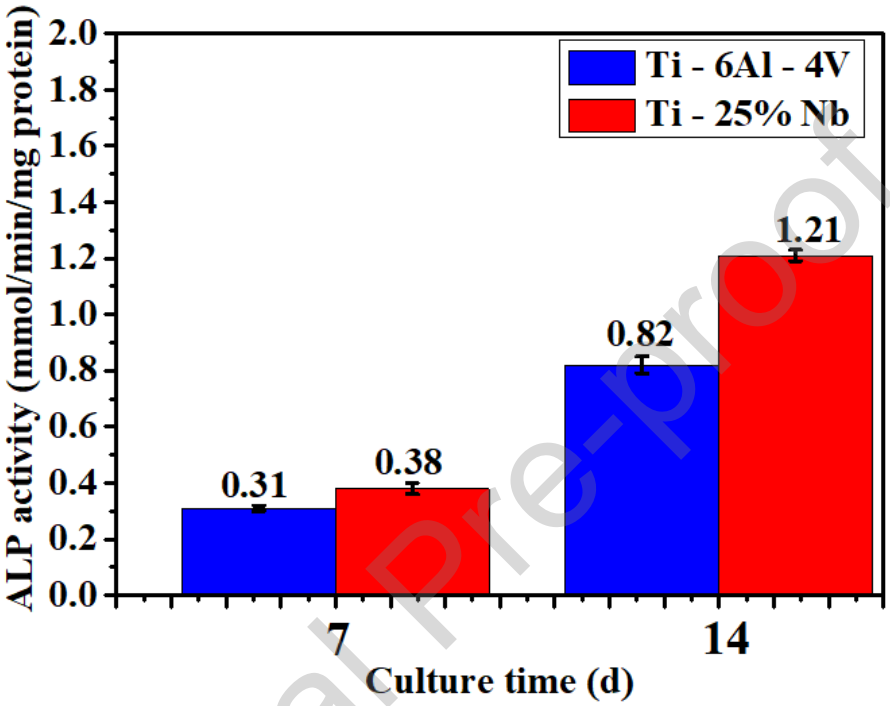

Fig.10. ALP activity of Ti-6Al-4V standard implant and SLM fabricated Ti-25Nb alloy.

As shown in Fig.10, at the end of 7 days, the ALP activity on Ti25Nb and Ti-6Al-4V is 0.38 and 0.31 mmol.min^{-1}.mg^{-1}, respectively. However, by the end of the 14th day, ALP activity on the former increases significantly ($p < 0.01$) to 1.21 mmol.min^{-1}.mg^{-1} but that on the latter is only 0.40 mmol.min^{-1}.mg^{-1} lesser. Since exposure of the alloy surfaces to the cell culture media will lead to hydrolysis of the constituent metals and evolution of hydrogen ions, the pH will decrease. However, the improved ALP activity on both alloys indicates that the solution remains alkaline (pH ≈ 7.45 -7.42) for the duration of the ALP activity evaluation.

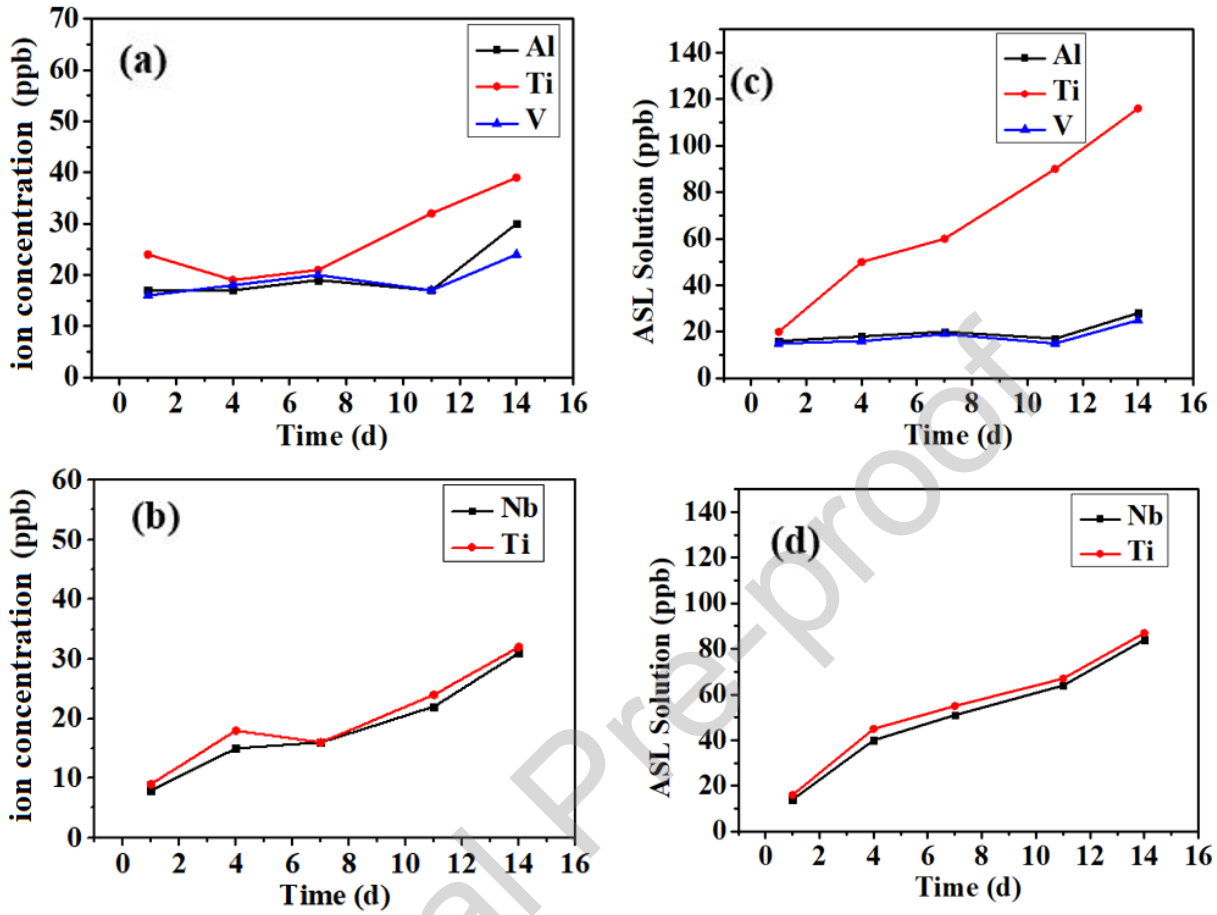

Fig.11 (a) Ion release of Ti-6Al-4V alloy in Hank's solution, (b) ion release of Ti-25Nb alloy in Hanks's solution, (c) ion release of Ti-6Al-4V implant in ASL media, (d) ion release of Ti-25Nb alloy in ASL media.

Next, the chemical stability of the two alloys is studied by evaluating their ion release kinetics in Hank's and ASL solutions for 14 days. Fig. 11(a) and (b) display the ion concentration of Ti-6Al-4V surface as a function of the exposure duration to Hank's and ASL solutions, respectively. In Hank's solution, the concentration of Ti^{+2}, Al^{+3} and V^{+1} ions is 20 ppb up to 7 days. Thereafter, the concentration of Ti^{+2} ions steeply increases to 38 ppb at the end of 14 days. However, the concentration of other two ions only increase to 30 ppb. In contrast, the concentration of Ti^{+2} ions increase monotonically with duration of exposure to ASL solution and

is ~116 ppb at the end of 14 days, whereas those of Al^{+3} and V^{+3} increase marginally to 20 ppb. Fig. 11(c) and (d) display the ion concentration of Ti-25Nb surface as a function of the exposure duration to Hank's and ASL solutions, respectively. In the both solutions, the ion release rates steadily increase but the final concentration of Ti^{+2} is only 30 ppb and 86 ppb in the two solutions, which is comparatively lower than that of Ti-6Al-4V. In addition, the magnitude and rate of increase of Nb^{+2} ion concentration is also similar to that of Ti^{+2} ions. However, while the concentration of Nb^{+2} is significant after 14 days, it is non-toxic and bio-compatible, unlike Al^{+3} and V^{+3} ions. The differences in the release of Ti^{+2} ions in Ti-25Nb and Ti-6Al-4V can be attributed to the nature of its passive films. In Ti-6Al-4V, all metal oxides apart from TiO_2 are unstable and allow the easy diffusion of Ti^{+2} ions through them. In contrast, Nb_2O_3 and Nb_2O_5, on the surfaces of Ti-25Nb, are highly stable films, which mitigate the release of metal ions in the solution.

Based on these results, it is evident that SLM fabricated Ti-25Nb alloy is more promising than Ti-6Al-4V for implant applications, given its better bio-tribocorrosion resistance, cell viability and ALP activity. In addition, it releases lesser Ti^{+2} ions in different types of SBF compared to that of Ti-6Al-4V, which otherwise leads to inflammation of tissues. Further studies are needed to investigate the antibacterial abilities of Ti-25Nb and the further improvement of its biocompatiblity with post-processing heat treatments and surface treatments such as ultrasonic shot peening and laser ablation.

4. Conclusions

Bio-tribocorrosion resistance of novel Ti-25Nb alloy was evaluated in normal human physiological environment and inflammatory conditions and their results are benchmarked with

commercial Ti-6Al-4V implant. From the detailed investigation the main conclusions are summarized as follows:

1) The microstructure of the conventional Ti-6Al-4V implant was found to have a coarse equiaxed structure, but the SLM-fabricated Ti-25Nb alloy had a fine lamellar Widmanstätten structure, despite the fact that both alloys contained α+β phases.
2) According to the findings of the bio-tribological study, the presence of Nb in Ti-25Nb implant offered improved re-passivation potential and demonstrated stronger wear resistance than the Ti-6Al-4V implant. Nevertheless, high cooling rate of SLM fabrication process induced high compressive residual stresses which offered greater resistance to ploughing. But the poor tribological resistance of commercial Ti-6Al-4V implants produced conventionally might be explained by little residual stress and the unstable Al_2O_3 and V_2O_5 passive films.
3) Improved tribological resistance of Ti-25Nb implant could be attributed the compactness of strong Nb_2O_5 passive film which attenuated the contact shear stress at the sliding interface and reduced the friction.
4) Results of biocompatibility analyses revealed that the Ti-25Nb implant showed better cell adhesion, cell spreading, osteogenic differentiation, cell proliferation and improved ALP activity compared to that of Ti-6Al-4V implant. The improved bionic function of Ti-25Nb implant was attributed to the negligible toxicity of Nb_2O_5 passive films.
5) Ion release test showed that Ti-25Nb implants release ions more slowly even under highly inflammatory conditions, suggesting that they could be employed as a suitable replacement for Ti-6Al-4V implants.

Acknowledgements

RLN acknowledges funding and support from the Start-up Research grant (SRG/2020/000095) of the Science and Engineering Research Board, DST, GoI.

References

1. E. Farghadany, A. Zarei-Hanzaki, H. R. Abedi, D. Dietrich, and T. Lampke, The strain accommodation in Ti–28Nb–12Ta–5Zr alloy during warm deformation, Mater. Sci. Eng. A. 592 (2014) 57-63.
2. F. Haftlang, A. Zarei-Hanzaki & H. R. Abedi, The effect of nano-size second precipitates on the structure, apatite-inducing ability and in-vitro biocompatibility of Ti-29Nb-14Ta-4.5 Zr alloy, Mater. Sci. Eng. C. 109 (2020) 110561.
3. V., Chakkravarthy, S.P. Jose, M. Lakshmanan, P. Manojkumar, R. Lakshmi Narayan, and M. Kumaran, Additive manufacturing of novel Ti-30Nb-2Zr biomimetic scaffolds for successful limb salvage, Mater. Today: Proc. 64 (2022) 1711-1716.
4. V. Chakkravarthy, J. P. Oliveira, Anisa Mahomed, Nan Yu, P. Manojkumar, M. Lakshmanan, L. Zhang, V. Raja, S. Jerome, T.R. Prabhu, and R.L. Narayan, Effect of abrasive water jet peening on NaCl-induced hot corrosion behavior of Ti–6Al–4V, Vacuum 210 (2023) 111872.
5. F. Haftlang, A. Zarei-Hanzaki, H.R. Abedi, J. Málek, E. Farabi, and H. Beladi, Outstanding mild wear performance of Ti–29Nb–14Ta–4.5 Zr alloy through subsurface grain refinement and supporting effect of transformation induced plasticity, Met. Mater. Int. 26 (2020) 467-476.
6. F. Haftlang, A. Zarei-Hanzaki, and H.R. Abedi, In-situ frictional grain refinement of Ti–29Nb–14Ta–4.5 Zr bio-alloy during high-speed sliding wear, Mater. Lett. 261 (2020) 127083.

7. P.A. Mouthuy, S.J. Snelling, S.G. Dakin, L. Milković, A.Č. Gašparović, A.J. Carr, and N. Žarković, Biocompatibility of implantable materials: an oxidative stress viewpoint, Biomaterials 109 (2016) 55-68.
8. A. L. Martinez, M. Saugo, D. O. Flamini, and S. B. Saidman, Enhancing the corrosion behavior of Ti–6Al–4V and Nitinol alloys by simple chemical oxidation in H_2O_2. Materials Chemistry and Physics 295 (2023) 127069.
9. M.A.H. Gepreel, and M. Niinomi, Biocompatibility of Ti-alloys for long-term implantation, J. Mech. Behav. Biomed. Mater. 20 (2013) 407-415.
10. F. Rajabi, A. Zarei Hanzaki, H. R. Abedi, H. Hoseiny, A. Najdahmadi, and E. Bertrand, Microstructure evolution and corrosion behavior of Ti-29Nb-13Ta-4.6 Zr nano-biocomposite fabricated by friction stir processing in simulated body fluid solution, Mater. Res. Express. 6 (2019) 105414.
11. F. Haftlang, A. Zarei-Hanzaki, H.R. Abedi, and M.A. Kalaei, Tribological Performance and Electrochemical Behavior of Ti-29Nb-14Ta-4.5 Zr Alloy in Simulated Physiological Solution, Adv. Eng. Mater. 22 (2020) 1900758.
12. A. N. Jinoop, S. Kanmani Subbu, and R. Arockia Kumar, Mechanical and microstructural characterisation on direct metal laser sintered Inconel 718, Int. J. Addit. Subtract. Mater. Manuf. 2 (2018) 1-12.
13. C. P. Paul, A. N. Jinoop, A. Kumar, and K. S. Bindra. Laser-based metal additive manufacturing: technology, global scenario and our experiences. Trans. Indian Natl. Acad. Eng. (2021) 1-14.
14. S.K. Nayak, A.N. Jinoop, C.P. Paul, V.A. Kumar, D. Subburaj, R. Singh, and K.S. Bindra, On the hot isostatic pressing of Inconel 625 structures built using laser powder bed fusion at higher layer thickness, J. Adv. Manuf. Technol. 120 (2022) 4065-4078.
15. K.S.N.S. Idury, V. Chakkravarthy, and R. L. Narayan. Mechanical behavior of laser powder bed fusion processed inconel 625 alloy. Trans. Indian National Acad. Eng. (2021) 1-16.
16. S. P, Kumar, V. Chakkravarthy, A. Mahalingam, R. Rajeshshyam, N. Sriraman, P. Marimuthu, R. Lakshmi Narayan, and P. Dinesh Babu, Investigation of Crystallographic Orientation and Mechanical Behaviour in Laser-Welded Stainless Steel 316L Additive Components, Trans. Indian Inst. Met. (2022) 1-9.

17. S. Huang, R.L. Narayan, J.H. Kuan Tan, S.L. Sing, and W.Y. Yeong. Resolving the porosity-unmelted inclusion dilemma during in-situ alloying of Ti34Nb via laser powder bed fusion, Acta Mater. 204 (2021) 116522.
18. S. Huang, P. Kumar, W.Y. Yeong, R.L. Narayan, and U. Ramamurty, Fracture behavior of laser powder bed fusion fabricated Ti41Nb via in-situ alloying, Acta Mater. 225 (2022) 117593.
19. A. Brończyk, P. Kowalewski, and M. Samoraj, Tribocorrosion behaviour of Ti6Al4V and AISI 316L in simulated normal and inflammatory conditions, Wear 434 (2019) 202966.
20. H. Qu, J. Li, F. Zhang, and J. Bai, Anisotropic cellular structure and texture microstructure of 316L stainless steel fabricated by selective laser melting via rotation scanning strategy, Mater. Des. 215 (2022) 110454.
21. K. Guan, Z. Wang, M. Gao, X. Li, and X. Zeng, Effects of processing parameters on tensile properties of selective laser melted 304 stainless steel, Mater. Des. 50 (2013) 581-586.
22. Z. Zhang, B. Chu, L. Wang, and Z. Lu, Comprehensive effects of placement orientation and scanning angle on mechanical properties and behavior of 316L stainless steel based on the selective laser melting process. J. Alloys Compd. 791 (2019) 166-175.
23. A. Leicht, Y. Cheng-Han, V. Luzin, U. Klement, and E. Hryha, Effect of scan rotation on the microstructure development and mechanical properties of 316L parts produced by laser powder bed fusion, Mater. Charact. 163 (2020) 110309.
24. H. Qu, J. Li, F. Zhang, and J. Bai, Anisotropic cellular structure and texture microstructure of 316L stainless steel fabricated by selective laser melting via rotation scanning strategy, Mater. Des. 215 (2022) 110454.
25. Instrument Care, Cleaning, Maintenance and Sterilization Instructions, Zimmer Biomet, (2021) 3455.1
26. Trabecular Metal and Tapered Screw-Vent Systems A Restorative Manual, Zimmer Biomet.

27. V. Teixeira, M. Andritschky, W. Fischer, H.P. Buchkremer and D. Stover, Effects of deposition temperature and thermal cycling on residual stress state in zirconia-based thermal barrier coatings, Surf. Coat. Technol. 120 (1999) 103–111
28. T. Murotani, H. Hirose, T. Sasaki and K. Okazaki, Study on stress measurement of PVD-coating layer. Thin Solid Films, 377 (2000) 617–620
29. U. Welzel, J. Ligot, P. Lamparter, A.C. Vermeulen and E.J. Mittemeijer, Stress analysis of polycrystalline thin films and surface regions by X-ray diffraction, J. Appl. Crystall. 38 (2005) 1–29
30. C.M. Moreno, J.M. Sanchez, L.C. Ardila and J.M.M. Aldareguia, Determination of residual stresses in cathodic arc coatings by means of the parallel beam glancing X-ray diffraction technique, Thin Solid Films 518 (2009) 206–222
31. Q. Luo and A.H. Jones High-precision determination of residual stress of polycrystalline coatings using optimised XRD-sin2ψ technique, Surf. Coat. Technol. 205 (2010) 1403–1408
32. S. Pilz, T. Gustmann, F. Günther, M. Zimmermann, U. Kühn and A. Gebert, Controlling the Young's modulus of a ß-type Ti-Nb alloy via strong texturing by LPBF, Mater. Des. 216 (2022) 110516.
33. Y. Su, C. Liang, X. Sun, H. Zhang, Q. Liang, Y. Zheng, Y. Hao, R. Yang, D. Wang, D. Banerjee, and Y. Wang, Composition-dependent shuffle-shear coupling and shuffle-regulated strain glass transition in compositionally modulated Ti-Nb alloys, Acta Mater. (2023) 118697.
34. A. Takase, T. Ishimoto, R. Suganuma and T. Nakano, Lattice distortion in selective laser melting (SLM)-manufactured unstable β-type Ti-15Mo-5Zr-3Al alloy analyzed by high-precision X-ray diffractometry. Scr. Mater. 201 (2021) 113953.

35. J. Xu, C. Liu, J. Wu, H. Li, B. Qi, D. Zhang, Y. Zhang, Y. Zhao, and L. Zhou, New insight into the role of microscale residual stresses on initial corrosion behavior of Ti35 alloy. Corros. Sci. 206 (2022) 110491.
36. D.R. Ununе, G.R. Brown, and G.C. Reilly, Thermal based surface modification techniques for enhancing the corrosion and wear resistance of metallic implants: A review. Vacuum (2022) 111298.
37. V. Chakkravarthy, M. Lakshmanan, P. Manojkumar, and R. Prabhakaran. Crystallographic orientation and wear characteristics of TiN, SiC, Nb embedded Al7075 composite. Mater. Lett. 306 (2022) 130936.
38. E.A. Esfahani, O. Bukuaghangin, S. Banfield, Y. Vangölü, L. Yang, A. Neville, R. Hall, and M. Bryant, Surface engineering of wrought and additive layer manufactured Ti-6Al-4V alloy for enhanced load bearing and bio-tribocorrosion applications. Surf. Coat. Technol. 442 (2022) 128139.
39. L. Salas, J. Chávez, O. Jimenez, M. Flores-Jimenez, F. Alvarado-Hernandez, L. Olmos, J. Pérez-Alvarez, and M. Flores. Tribocorrosion and corrosion behavior of quaternary Ti-24Nb-xZr-ySn alloys in SBF. Mater. Lett. 283 (2021) 128903.
40. L.A. Alberta, J. Vishnu, Y. Douest, K. Perrin, A.M. Trunfio-Sfarghiu, N. Courtois, A. Gebert, T.O. Benoit and M. Calin, Tribocorrosion behavior of β-type Ti-Nb-Ga alloys in a physiological solution, Tribol. Int. (2023) 108325.
41. B. Rahmatian, H. M. Ghasemi, M. Heydarzadeh Sohi, and P. De Baets, Tribocorrosion and corrosion behavior of double borided layers formed on Ti-6Al-4V alloy: An approach for applications to bio-implants, Corros. Sci. 210 (2023) 110824.
42. B. Cheraghali, H. M. Ghasemi, M. Abedini, and R. Yazdi. Functionally graded oxygen-containing coating on CP-titanium for bio-applications: characterization, biocompatibility and tribocorrosion behaviour, J. Mater. Res. Technol. 21 (2022) 104-120.
43. S.W. Lee, K.S. Phillips, H. Gu, M. Kazemzadeh-Narbat and D. Ren, How microbes read the map: Effects of implant topography on bacterial adhesion and biofilm formation, Biomaterials 268 (2021) 120595.
44. C. Prakash, S. Singh, S. Ramakrishna, G. Królczyk, and C.H. Le, Microwave sintering of porous Ti–Nb-HA composite with high strength and enhanced bioactivity for implant applications, J. Alloys Compd. 824 (2020) 153774.

Author credit statement

V Chakkravarthy – Writing original draft and experimental investigation.

P Manoj kumar - Data curation and Formal analysis.

M. Lakshmanan – Conceptualization.

K. Eswar Prasad- Resources and investigation.

Rucha Dafale- Characterization and investigation.

V. Chitra Vadhana- Methodology, writing and data curation.

R.L. Narayan- Supervision, Funding acquisition, Project administration, Writing - review & editing.

Declaration of interests

☒ The authors declare that they have no known competing financial interests or personal relationships that could have appeared to influence the work reported in this paper.

Highlights

- A novel Ti-25Nb bioactive implant was developed via selective laser melting route.
- Nb offers rapid repassivation potential through formation of Nb_2O5 passive film.
- Compared to Ti-6Al-4V, Ti-25Nb exhibits superior osseointegration
- Improved focal adhesion of MC3T3-E1 pre-osteoblast cells was observed on Ti-25Nb
- Improved Alkaline phosphatase activity (ALP) of Ti-25Nb suggests that it is bio-inert.

Comparing bio-tribocorrosion of selective laser melted Titanium-25% Niobium and conventionally manufactured Ti-6Al-4 V in inflammatory conditions

Chakkravarthy, Vijayavarman

2023-04-10

Chakkravarthy V, Manojkumar P, Lakshmanan M, et al., (2023) Comparing bio-tribocorrosion of selective laser melted Titanium-25% Niobium and conventionally manufactured Ti-6Al-4v in inflammatory conditions. Journal of Alloys and Compounds, Volume 952, August 2023, Article number 169852

https://doi.org/10.1016/j.jallcom.2023.169852